International Journal of Thermophysics (2020) 41:51
https://doi.org/10.1007/s10765-020-02631-w

Nanoparticle-Stabilized Lattices of Topological Defects in Liquid Crystals

Apparao Gudimalla[1,2] · Marta Lavrič[2] · Maja Trček[2] · Saša Harkai[2] · Brigita Rožič[2] · George Cordoyiannis[3] · Sabu Thomas[4,5] · Kaushik Pal[6] · Zdravko Kutnjak[1,2] · Samo Kralj[2,7]

Received: 27 August 2019 / Accepted: 21 February 2020 / Published online: 4 March 2020

Abstract

We present a review of nanoparticle (NP) stabilized lattices of topological defects (TDs) in liquid crystals (LCs). We focus on conditions for which chiral liquid-crystalline blue phases and twist-grain boundary A phases might be stable in bulk LCs. These phases exhibit lattices of disclinations and dislocations corresponding to line TDs in orientational and translational LC order, respectively. NPs of appropriate size and surface coating can assemble in the cores of defects and stabilize metastable or increase the temperature range of already stable lattices of TDs. The stabilization is achieved by the universal defect core replacement and adaptive defect core targeting mechanisms. Representative experiments revealing these phenomena and potential applications are discussed.

Keywords Disclinations · Dislocations · Liquid crystals · Nanoparticles · Topological defects

✉ Samo Kralj
samo.kralj@ijs.si

[1] Jožef Stefan International Postgraduate School, Jamova 39, 1000 Ljubljana, Slovenia

[2] Condensed Matter Physics Department, Jožef Stefan Institute, Jamova 39, 1000 Ljubljana, Slovenia

[3] Faculty of Mechanical Engineering, Czech Technical University in Prague, 16600 Prague 6, Czech Republic

[4] International and Inter-University Center for Nanoscience and Nanotechnology, Mahatma Gandhi University, Kottayam, Kerala, India

[5] School of Chemical Sciences, Mahatma Gandhi University, Kottayam, Kerala, India

[6] Department of Nanotechnology, Bharath University, BIHER Research Park, 173 Agharam Road, Selaiyur, Chennai, Tamil Nadu 600073, India

[7] Faculty of Natural Sciences and Mathematics, University of Maribor, Koroška 160, 2000 Maribor, Slovenia

Abbreviations

NP	Nanoparticle
TD	Topological defect
LC	Liquid crystal
BP	Blue phase
BPI, BPII, BPII	Blue phase I, blue phase II, blue phase III
TGB	Twist-grain boundary
N	Nematic
Sm*A*	Smectic-A
Sm*C*	Smectic-C
Cr	Crystal
N^*	Chiral nematic
I	Isotropic phase
N_L^*	Chiral line liquid
LGG	Landau–de Gennes–Ginzburg
DCR	Defect core replacement
ADCT	Adaptive defect core targeting
Au NPs	Gold nanoparticles
CdSe	Cadmium selenide
CdSSe	Cadmium sulfide selenide
CE8	S-(+)-[4-(2′-methylbutyl) phenyl 4′-*n*-octylbiphenyl-4-carboxylate]

1 Introduction

Soft nanocomposites consisting of liquid-crystalline (LC) [1] matrices hosting nanoparticles (NPs) comprise a research topic of high interest [2, 3]. In such systems, both the individual and combined properties of the constituents are exploited. These nanocomposites [4] often display either greatly enhanced or qualitatively new features with respect to pure LC matrices.

The key reasons for the intense interest in studying the properties of soft nanocomposites are as follows. First, the diverse LC configurations [5] display a plethora of physical phenomena that could be exploited in developing various applications [6]. Furthermore, LC matrices exhibit a unique combination of liquid character, optical anisotropy, and softness. The liquid LC character enables a relatively simple preparation of LC–NP mixtures and phase separation phenomena can be avoided with careful choice of the latter. Diverse combinations of LC configurations and NP dopants (with diversity in their chemical structure, NP size and shape variations, surface treatments, etc.) enable rich complexity and new emerging phenomena, which could be exploited in various applications [7]. LC optical anisotropy allows to experimentally probe structural and phase transition properties using simple (e.g., polarizing optical microscopy) experimental setups. Finally, softness refers to the capability of relatively strong responses to even weak perturbations [8].

The origin of softness is the continuous symmetry-breaking [5, 8] via which most LC phases, the so-called mesophases, are reached. The transition between

different mesophases could be described by an order parameter field, consisting of two qualitatively different contributions: the *amplitude* field and the *symmetry-breaking* (also referred to as the *gauge*) field. The first component determines the strength of a newly established order, exhibiting a single equilibrium value for given conditions. On the contrary, the second component describes a symmetry-breaking choice among an infinite degenerate set of possible options. Firstly, this degeneracy is reflected in easily excitable Goldstone fluctuations that introduce softness to LC phases [8]. The symmetry-breaking field endows LCs with a sensitive structural "vision" of conditions in different parts of the LC body. They could even give rise to long-range forces between immersed objects, such as NPs. Secondly, owing to degeneracy, the symmetry-breaking fields could be in general frustrated, giving rise to topological defects (TDs) [9, 10]. In most cases, TDs appear in localized regions where the relevant symmetry-breaking field is not uniquely defined. This singularity typically gives rise to local melting of the amplitude field. The local region, where the amplitude is substantially suppressed, defines the core of a defect. The correlation length of the amplitude field determines the characteristic linear size of a defect's core.

The symmetry-breaking phase transitions, and their unavoidable consequence, TDs, are ubiquitous in nature [11]. The resulting phenomena are intertwined with universal behaviors. Namely, the topological origin of TDs, which is "blind" for microscopic details, makes this area of research strongly interdisciplinary [11], and consequently of interest for all branches of physics (i.e., including particle physics, condensed matter, and cosmology). To emphasize the potential importance of physics of TDs, we remind that *fields* could represent basic entities of nature [12]. In this case, topologically protected TDs might represent *fundamental particles*, as first suggested by Skyrmy [13].

In general, TDs are energetically costly. For this reason structures dominated by TDs are relatively rarely realized in bulk equilibrium phases. In LCs, they could be stabilized by the inherent chirality of LC molecules [5]. For strong enough chiralities, LC phases exhibiting lattices of line TDs in orientational or translational order could exist [5]. These are realized in blue phases (BPs) [14, 15] and smectic twist-grain boundary phases (TGBs) [16, 17]. Henceforth, we focus on these phases and the impact of NPs on their stability. NPs could have a strong impact on such phases depending on their concentration, characteristic linear size, shape, surface treatment, and NP–LC interaction.

In this review, we present how NPs could be exploited to stabilize lattices of TDs in LCs. The structure of the paper is as follows. In Sect. 2, main LC phases are presented, focusing on BPs and TGBs. The structure of line defects present in these phases is described. In Sect. 3, the impact of NP–LC interaction on TDs in LC orientational and translational order is discussed. In Sect. 4, we report on experimental results that reveal the impact of NPs on phase transition behavior and stability of BPs and TGBs, followed by conclusions.

2 Liquid Crystal Structures Hosting Line Defect Lattices

In this section, the common phases exhibited by thermotropic LCs are presented. We first present main defectless (non-frustrated) thermotropic LC phases, exhibiting orientational and translational ordering. Orientational and translational order parameters are introduced describing the simplest structures in these orderings. Line TDs present in these structures and chirality-driven thermodynamically stable frustrated LC configurations hosting such line defects are described.

2.1 Defectless Liquid Crystal Phases

The mechanical and symmetry properties of LC phases are intermediate between those of a conventional isotropic liquid and those of a solid crystal. Most common LC configurations, referred to as *thermotropic, lyotropic* and *polymeric* LCs [5, 18–21], are shown in Fig. 1. We restrict our focus on thermotropic LC phases that are reached on varying temperature. Furthermore, we consider only LCs consisting of rod-like molecules. A typical sequence of phases met in non-chiral LCs on decreasing temperature T from the isotropic phase is illustrated in Fig. 2.

The nematic uniaxial phase is the simplest LC structure exhibiting only the long-range orientational order. The latter is at the mesoscopic level commonly described by the traceless and symmetric nematic tensor order parameter [5]

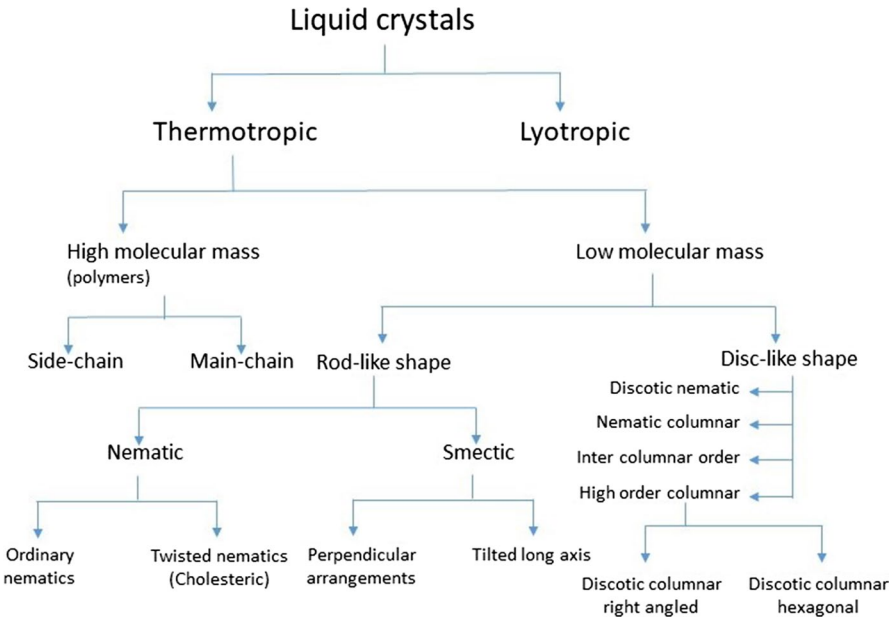

Fig. 1 Classification of liquid crystals

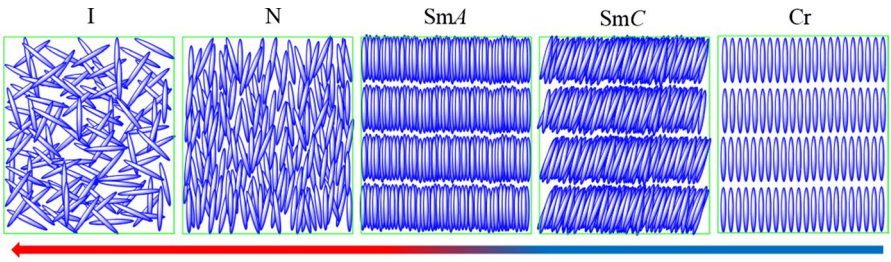

Fig. 2 Typical phases of non-chiral LCs on decreasing temperature from the isotropic (*I*), i.e., ordinary liquid-like phase, going through the nematic (*N*), smectic-A (Sm*A*), smectic-C (Sm*C*), and finally reaching the crystal (Cr) phase

$$\underline{Q} = \sum_{i=1}^{3} s_i \vec{e}_i \otimes \vec{e}_i,$$

where s_i are $\underline{Q}$ eigenvalues (the amplitude fields), and $\vec{e}_i$ its eigenvectors (the symmetry-breaking fields). In the case of biaxial states, all the eigenvalues are different. In bulk the orientational order for most LCs is uniaxial. In this case, $\underline{Q}$ is expressed as [5]

$$\underline{Q} = s\left(\vec{n} \otimes \vec{n} - \underline{I}/3\right), \tag{1}$$

where $\vec{n}$ is the nematic director (symmetry-breaking) field, s is the nematic order parameter (amplitude) field, and $\underline{I}$ stands for the unit tensor. The unit vector field $\vec{n}$ points along the average local orientation of a rod-like LC molecule, where the states $\pm\vec{n}$ are physically equivalent. The degree of order is described by the uniaxial order parameter (amplitude) field s, where $s \in \left[-\frac{1}{2}, 1\right]$. In the bulk equilibrium the nematic order is spatially homogeneous, i.e., $s > 0$ and $\vec{n}$ points along a symmetry-breaking direction.

On further decreasing T, smectic phases typically appear. In addition to orientational order, they also possess the positional quasi-long-range order. In equilibrium, common smectic phases consist of a stack of parallel and equidistant smectic layers. Depending on the molecular order in layers, one distinguishes among different smectic phases. The simplest is the Sm*A* phase, where LC molecules tend to be aligned parallel to the smectic layer normal. In the bulk Sm*A* equilibrium, the layers are stacked along the spatially homogeneous director field orientation. In the simplest modeling, the layer order is described by the mesoscopic order parameter field [5, 22]

$$\psi = \eta e^{i\phi}, \tag{2}$$

where η and ϕ represent the translational amplitude and symmetry-breaking field, respectively. This order parameter field approximately describes the mass density spatial variation

$$\rho = \rho_0(1 + \psi + \psi^*),$$

where ρ_0 is a constant. In bulk equilibrium η is spatially homogeneous, $\phi = q_0\vec{n}.\vec{r}$, and the periodicity $q_0 = 2\pi/d_0$ determines the smectic layer spacing d_0.

2.2 LC Phases with Line Defects

If LC order is frustrated, topological defects could be present [9, 23]. In bulk, this could be realized in strong enough chiral LCs. In such cases, lattices of line defects are introduced in the orientational and translational LC order. In the following, we present the simplest defects in (i) orientational and (ii) translational order, which are commonly referred to as (i) disclinations and (ii) dislocations. Afterward we describe stable bulk LC phases hosting these defects.

2.2.1 Line Defects

Disclinations in nematic order correspond to points where $\vec{n}$ is not uniquely defined. The most common are $m = 1/2$ and $m = -1/2$ disclinations [24, 25], characterized by the winding number m. The latter determines the number of reorientations of $\vec{n}$ on encircling a line defect counter clockwise. Half integers are possible due to the $\pm\vec{n}$ invariance. Their typical nematic director structure is as shown in Fig. 3. Note that in nematic LCs the disclination core [26, 27] is in reality strongly biaxial in order to avoid the presence of a singularity at the center of the defect core.

The simplest defects in translational order are screw and edge dislocations [5, 28–30] that are schematically depicted in Fig. 4. They exhibit discontinuities in the layer order (i.e., in the symmetry-breaking phase field ϕ). In the center of these defects, the amplitude of the smectic order parameter is melted ($\eta = 0$). Detailed mesoscopic structures described by order parameter fields ψ and $\underline{Q}$ of elementary screw and edge disclinations are given in [29, 30], respectively.

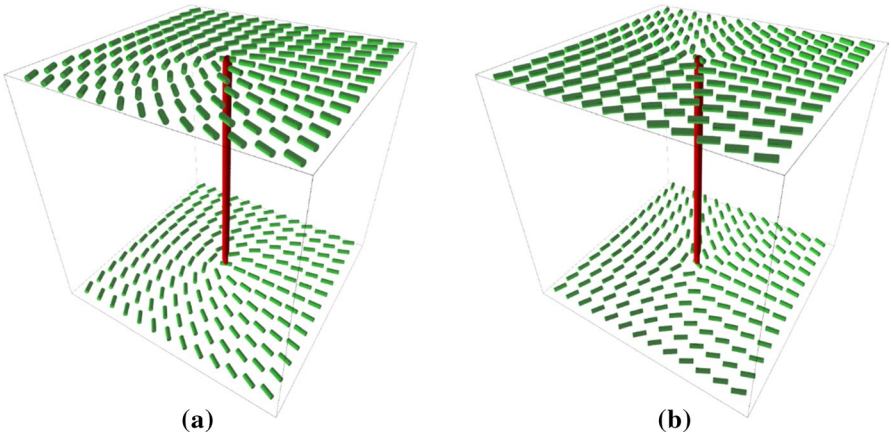

Fig. 3 The nematic (a) $m = 1/2$ and (b) $m = -1/2$ disclination

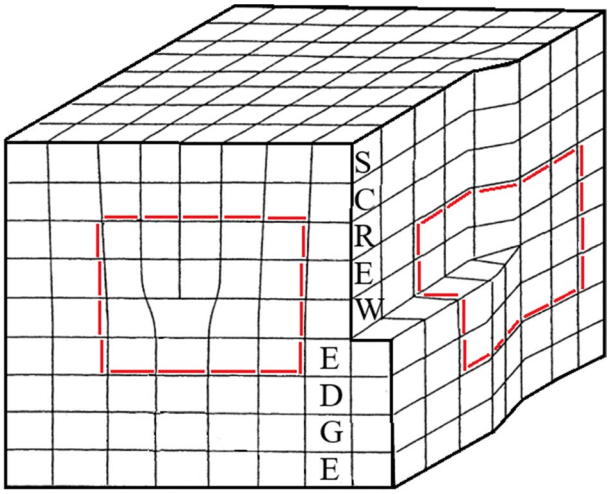

Fig. 4 Schematic sketch of an edge and screw dislocation

In general, structures exhibiting lattices of line defects are not stable due to the energetically costly defect cores. A simple and efficient way to stabilize these lattices of defects is to introduce chirality into the system, which can stabilize lattice of defects both in nematic and smectic order. We limit our review to BP [14, 15] and TGB_A [16, 17] structures, in which lattices of $m = -1/2$ disclinations and screw dislocations are stable, respectively. Note that TGB_A refers to a structure of grain boundaries separating slabs of Sm*A* order.

Note that in chiral LCs the nematic (*N*) phase is replaced by the chiral nematic (N^*), also referred to as cholesteric [5]. This phase consists of cross-sections exhibiting nematic order, which are uniformly twisted along the perpendicular direction. For a strong chirality, different BP configurations could be introduced between the isotropic (*I*) and chiral nematic (N^*) phase, and/or the TGB_A phase could intervene in a narrow temperature window separating the defectless N^* and Sm*A* phases. In the following, we summarize the main features of BP and TGB_A configurations.

2.2.2 Blue Phases

Blue phases were discovered by Reinitzer already in the 1888 [31]. However, they started to attract research interest in 1960s. BPs are highly fluid self-assembled three-dimensional cubic defect structures [32]. Three distinct thermodynamic BP phases can exist (see Fig. 5), which commonly appear in a narrow (from 1 K to 3 K) temperature interval between the *I* and the N^* phases [33]. BPs consist of "double-twist" cylinders that tend to be arranged mutually perpendicularly. The double-twist structure, which is energetically more favorable than a single twist [34–36] realized in N^*, is illustrated in Fig. 6. In order to realize double-twist configurations, a lattice of $m = -1/2$ disclinations needs to be introduced due to topological reasons. The disclinations form a cubic lattice, where the characteristic lattice linear scale

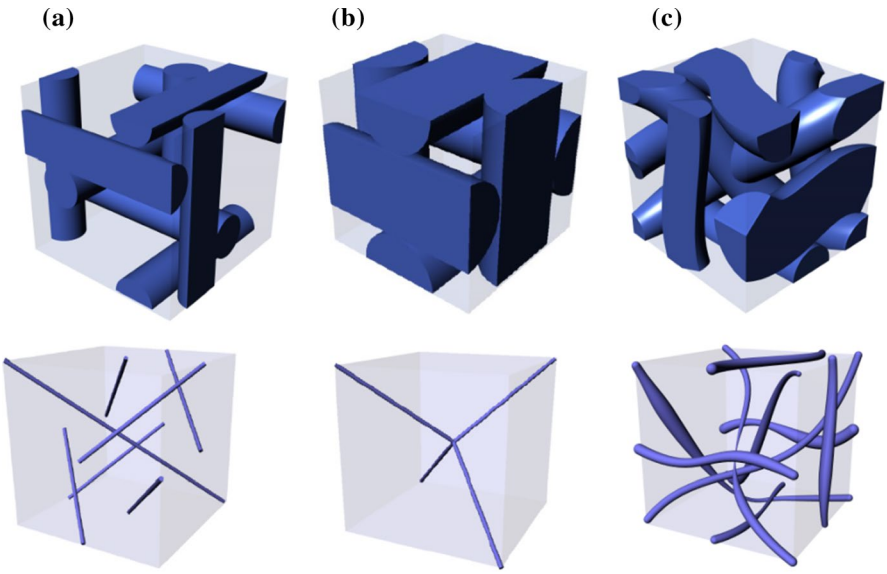

Fig. 5 The packing of double-twist cylinders (top panel) and the structure of disclinations (bottom panel) are presented, corresponding to (a) BPI, (b) BPII, (c) BPIII

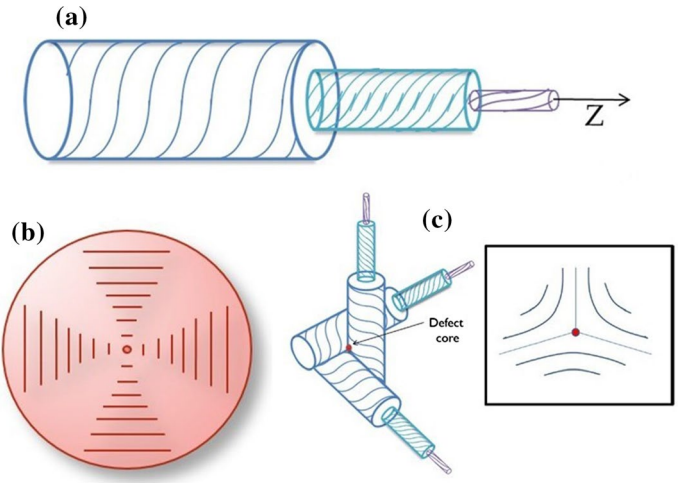

Fig. 6 (a) Schematic presentation of a double-twist cylinder aligned along the z-coordinate. The lines indicate the nematic director field. (b) The double-twist director field in the (x, y) plane is indicated, where $\vec{n}$ points along the z-direction at the symmetry axis. (c) Double-twist cylinders topologically enforce $m = -1/2$ disclinations

is typically in the range of several hundred nm [34]. The BPs are classified into BPI, BPII, and BPIII structures, which are shown in Fig. 5. BPI and BPII display a relatively high degree of translational order. BPI exhibits a cubic body-centered

structure, while BPII has a simple cubic unit (i.e., the double-twist cylinders are packed in the cubic lattice) [37, 38]. On the contrary, BPIII is characterized by a random network of disclination lines [39]. Consequently, BPIII possesses macroscopically the same symmetry as the *I* phase [38].

In the early LC-BP research, the narrow stability range of these phases was always puzzling and comprised a challenge for interpretation [15]. In the pioneering work by Meiboom et al. [14], the stability of BPs was explained using a simple Oseen–Frank elasticity. Different types of BP temperature ranges could be well explained by using Meiboon's defect model [40].

Due to the narrow temperature stability range, BPs for a long time attracted interest only for fundamental studies. However, with time the scientific community realized the BPs potential for various applications in emerging technologies [41] such as three-dimensional lasers, tunable photonic crystals, and fast optical displays [42–45]. This has initiated extensive research efforts in the last decades to increase their temperature stability range. Several strategies such as chiral doping, polymer, and NP stabilization, as well as long-timescale preservation in supercooled state, are exploited for the stabilization of BPs in wider temperature ranges [34, 46–64].

2.2.3 Twist-Grain Boundary Phases

Chirality favors twist-like configurations, which are incompatible with the smectic layer-type configuration. Consequently, for large enough chirality lattices of screw disclinations could appear in order to energetically compromize the conflicting twist elastic deformations and smectic layer order. A typical TGB_A structure is shown in Fig. 7. It consists of blocks of bulk-like smectic order, where the neighboring blocks are twisted for a finite angle. This twist is enabled by a lattice of screw dislocations that reside in the so-called *grain boundaries*.

Note that TGB_A was predicted based on the mathematical analogy between smectic LCs and superconductors by de Gennes [22], who claimed that both phases could be described with a complex order parameter given by Eq. 2. He demonstrated an analogy between the N^*-Sm*A* and the normal metal–superconducting phase transition. By extending this analogy to structures possessing TDs, Renn and Lubensky

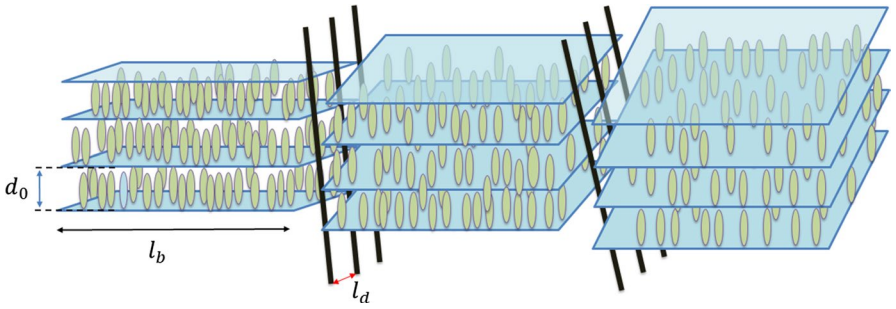

Fig. 7 Schematic presentation of the TGB_A structure. The width of smectic blocks is denoted by l_b, and the distance between vicinal screw dislocations by l_d

[16] proposed the TGB_A configuration [65] as the LC analogue to the Abrikosov flux phase appearing in type-II superconductors under external magnetic field. Twist penetrates the TGB_A structure via a lattice of screw dislocations that are roughly analogues of magnetic vortices [66] in the type-II superconducting phase. In the latter case, the Abrikosov flux lattice [66] is enforced by an external magnetic field.

Various types of TGB phases are distinguished based on the type of smectic ordering within the blocks. There exist three different ordered phases [67–69]: TGB_A, TGB_C, or TGB_C^* configurations, which exhibit in the blocks Sm*A*, Sm*C,* or SmC^* order, respectively [17, 70, 71].

Furthermore, the TGB_A phase could melt to a chiral line liquid just as the Abrikosov phase melts to a directed line liquid as predicted by Kamien and Lubensky [72]. They predicted the existence of a short-range TGB_A structure, corresponding to a liquid of screw dislocations. This phase is referred to as the chiral line liquid (N_L^*). Note that TGB_A and N_L^* are not thermodynamically distinct phases, because they share the same phase symmetry. Nevertheless, they differ in the range of translational order [68].

Experimentally, Goodby et al. discovered the TGB_A phase in 1989 [17, 70]. The optical properties of this phase are similar to the N^* phase. Srajer et al. [73] showed that the small-angle X-ray structure factor of this phase displays a continuous ring, which is consistent with the model of Renn and Lubensky [71]. The existence of the lattice of screw dislocations was confirmed by the freeze-fracture measurements of Ihn et al. [74]. The phase sequence N^*–TGB_A–Sm*A* was first detected by Lavrentovich et al. [75]. Finally, different TGB and N_L^* structures have been reported in Ref. [65, 68].

3 Mechanisms Stabilizing Defect Lattices

In the following, we present a minimal model to illustrate key mechanisms that generate and stabilize lattices of line defects. For this purpose, we use the Landau–de Gennes–Ginzburg (LGG) mesoscopic approach [5], where the nematic orientational and Sm*A* translational order are described by the uniaxial (for simplicity biaxial states are neglected) nematic tensor (see Eq. 1) and smectic complex (see Eq. 2) order parameter. Then we present mechanisms that generate line defects. Afterwards, we describe how these defects could be stabilized by appropriate NPs by means of DCR and ADCT mechanisms.

3.1 Free Energy Penalties

Using the LGG model, we express the free energy as the sum $F = \iiint f d^3\vec{r} + \iint f_i d^2\vec{r}$. The first integral is carried out over the LC body. The second integral is carried over the surfaces confining the LC body and NPs–LC interfaces, if NPs are present. The volume free energy density f is commonly expressed as the sum $f = f_c^{(n)} + f_e^{(n)} + f_c^{(s)} + f_e^{(s)}$ of nematic condensation ($f_c^{(n)}$), smectic condensation ($f_c^{(s)}$),

nematic elastic ($f_e^{(n)}$), and smectic elastic ($f_e^{(s)}$) contribution. Furthermore, f_i stands for the surface density interaction.

In the following, we introduce only the most essential free energy density terms, which are necessary to describe phases of our interest. We consider bulk samples, thus f_i determines the local NP–LC interface interactions. Furthermore, we describe LC structures in terms of nematic uniaxial order parameter and smectic order parameter given by Eqs. 1 and 2.

We express these contributions as [5]

$$f_c^{(n)} \sim a_n\left(T - T_n^*\right)s^2 - b_n s^3 + c_n s^4, \tag{3a}$$

$$\begin{aligned} f_e^{(n)} \sim L|\nabla s|^2 + K_1\left(\nabla.\vec{n}\right)^2 + K_2\left(\vec{n}.\nabla\times\vec{n} - q\right)^2 + K_3\left|\vec{n}\times\nabla\times\vec{n}\right|^2 \\ - K_{24}\nabla.\left(\vec{n}\nabla.\vec{n} + \vec{n}\times\nabla\times\vec{n}\right), \end{aligned} \tag{3b}$$

$$f_c^{(s)} \sim a_s\left(T - T_s^*\right)\eta^2 + b_s\eta^4 + c_s\eta^6, \tag{3c}$$

$$f_e^{(s)} \sim C_{\parallel}\left|\left(iq_0\vec{n} - \nabla\right)\psi\right|^2 + C_{\perp}\left|\left(\vec{n}\times\nabla\right)\psi\right|^2, \tag{3d}$$

$$f_i = wTr(\underline{Q} - \underline{Q}_i)^2. \tag{3e}$$

The quantities $a_n, b_n, c_n, a_s, b_s, c_s$ are temperature-independent Landau expansion coefficients, constants T_n^* and T_s^* roughly determine the critical temperatures below which the orientational and translational order condensate, respectively. The elastic LC properties are described by the representative nematic bare (i.e., temperature independent) elastic constant L, the temperature-dependent nematic splay (K_1), twist $\left(K_2\right)$, bend $\left(K_3\right)$, and saddle-splay $\left(K_{24}\right)$ nematic Frank constants, and the smectic compressibility ($C_{\parallel}$) and smectic bend ($C_{\perp}$) elastic constants. For conventional LCs these constants are positive in regions where nematic-type or SmA-type LC configurations are expected. The periodicity q introduces chirality into the system, and $q_0 = \frac{2\pi}{d_0}$ determines the equilibrium SmA layer spacing d_0. If NPs are present, then LC–NP local interactions are modeled by Eq. 3e. Here, Tr stands for the trace operation, $w > 0$ stands for the positive surface anchoring-wetting constant, and $\underline{Q}_i$ is the nematic order favored by the interface.

General tendencies enforced by these representative free energy density terms are described in Appendix.

3.2 Defect Stabilizing Mechanisms

We first discuss the conditions favoring BPs that are characterized by lattices of disclinations. The main phase-ordered competitor of BPs is the N^* phase. The latter is characterized by the twist nematic configuration, for which $f_e^{(n)} \sim 0$. On the

contrary, in BPs the first four elastic contributions in Eq. 3b are on average finite and positive. In addition, disclinations require melting (more exactly, the appearance of biaxial states) of the uniaxial nematic order in the cores of defects, introducing additional condensation penalty costs in BPs. The key BP-stabilizing term is thus the saddle-splay term for the positive value of K_{24}. Note that the elastic term weighted by K_{24} equals the Gaussian curvature G of a hypothetical local surface [5], whose surface normal is determined by $\vec{n}$. Therefore, $K_{24} > 0$ favors *double-cylinders* which are characterized by $G > 0$, decreasing the overall free energy. However, in between double-twist cylinders the LC structure exhibits regions where $G < 0$. Nevertheless, the free penalty in these regions is relatively small due to the presence of disclinations that, on average, decrease the amplitude of nematic local order so that the overall energy penalty balance favors the presence of disclinations.

In the case of smectic order, the smectic compressibility term represents the generator of dislocations. In order to show that we assume a spatially constant value of the smectic amplitude field η. Consequently, the minimization of the compressibility terms yields the condition

$$q_0 \vec{n} = \nabla \phi. \tag{4}$$

Applying the operation $\nabla\times$ on Eq. 4, one obtains $q_0 \nabla \times \vec{n} = \nabla \times \nabla \phi \equiv 0$, which leads in strongly chiral LCs to inequality, because of $\nabla \times \vec{n} \neq 0$. One could resolve this frustration either by melting the smectic order or by introducing dislocations. Note that in superconductors [71] one obtains a similar inequality, where $\vec{A}$ (which is related to the magnetic field $\vec{B} = \nabla \times \vec{A}$) plays the role of $\vec{n}$, and ϕ is the phase of the complex order parameter quantifying the condensation of the superconducting Cooper-pairs.

3.3 Nanoparticle-Driven Stabilization of TDs

Introducing NPs to LC structures hosting lattices of defects could efficiently enhance the stability of such structures. The key mechanisms enabling the stabilization are referred to as the defect core replacement (DCR) [46, 52, 54] and the adaptive defect core targeting (ADCT) [76] mechanisms.

3.3.1 DCR Mechanism

The DCR mechanism refers to the partial replacement of the relatively expensive TD cores volume with the volume of (partially) trapped NPs. Within the cores of disclinations and dislocations, the uniaxial nematic order and smectic order, respectively, are essentially melted [26, 29, 30]. This generally introduces relatively high energy costs in the respective condensation-free energy contributions. However, if NPs are trapped within the cores the free energy condensation penalty is reduced. In order to illustrate this, the condensation penalty $\Delta F_c^{(phase)}$ for introducing defects into a BP or TGB_A phase is estimated by

$$\Delta F_c^{(BP)} \sim \left| f_c^{(n)} \right| V_{def}, \tag{5a}$$

$$\Delta F_c^{(TGB)} \sim \left| f_c^{(s)} \right| V_{def}, \tag{5b}$$

where V_{def} estimates the total volume of defect cores within a system, and the condensation-free energy contributions are given in Eq. 3a, 3c. If NPs are trapped within the cores, they reduce the value of V_{def}.

Note that the above described mechanism is effective only when the NPs do not significantly distort the surrounding symmetry-broken order parameter field component (i.e., the nematic director field $\vec{n}$ or the smectic phase field ϕ), which is embodied in the universal ADCT mechanism. This mechanism refers to cases where the same NPs stabilize both lattices of disclinations and dislocations [76]. It incorporates the following characteristics: (i) NPs should slightly distort the symmetry-broken field of the LC structure in order to be attracted to a defect's core; (ii) if NPs are trapped within the cores they should not significantly distort the surrounding LC order; (iii) in order to have a universal impact on both disclinations and dislocations, NPs should have the potential to adapt to the structure of different environments. This last condition is met when NPs have an appropriate surface treatment [52, 54, 76].

3.3.2 ADCT Mechanism

The ADCT mechanism is effective only when the NP–LC interaction is moderate, i.e., neither too weak nor too strong. In order to estimate this condition in the nematic phase, the coupling at NP–LC interfaces is modeled by the free energy density term given by Eq. 3e. The appropriate regime enabling adaptivity is where the global interface and elastic penalty contributions are comparable. To obtain an estimate for such a condition [77] one compares the average free energy ΔF penalties in extreme cases, where either (i) elastic or (ii) surface interaction penalties are minimized. In the first case, the surface interaction contribution is maximal and is estimated by $\frac{\Delta F^{(i)}}{V} \sim \frac{N}{V} a_{NP} w \sim p \frac{a_{NP}}{v_{NP}} w$. Here, N stands for the number of NPs in the sample, a_{NP} and v_{NP} determine the average surface area and volume of a NP, and $p = \frac{N v_{NP}}{V}$ is the volume concentration of NPs. In the second regime, the interface penalties are negligible and the free energy penalties are dominated by the elastic deformations, which arise in order to accommodate NP–LC interfaces imposed order. It follows [77] that $\frac{\Delta F^{(ii)}}{V} \sim \frac{K}{l_{NP}^2}$, where K is the representative Frank elastic constant and $l_{NP} \sim \left(v_{NP}/p \right)^{1/3}$ is the average separation between essentially homogeneously dispersed NPs. The adaptive regime is estimated by imposing $\Delta F^{(i)} \sim \Delta F^{(ii)}$, yielding the condition

$$p \frac{a_{NP}}{v_{NP}} \frac{l_{NP}^2}{d_e} \sim 1, \tag{6a}$$

where $d_e \sim K/w$ defines the surface extrapolation length. For spherical NPs of radius r, it follows

$$\frac{p^{2/3} r}{d_e} \sim 1. \tag{6b}$$

For example, this condition is fulfilled for $w \sim 10^{-6}\,\mathrm{J{\cdot}m^{-2}}$ in case of conventional LCs [5] (i.e., $K \sim 10^{-12}\,\mathrm{J{\cdot}m^{-2}}$), spherical NPs of radius $r \sim 10$ nm and concentration $p \sim 0.001$.

It is noteworthy that lattices of defects could be also stabilized by other mechanisms, e.g., by effectively enhancing the chirality strength of the system [32]. This could be achieved by using appropriate chiral dopants.

4 Experimentally Observed Nanoparticle-Driven Stabilization

In the following, we first present experimental evidences [46, 52–54, 57, 58, 76–81] demonstrating the efficiency of the DCR and ADCT mechanisms in stabilizing lattices of line defects in different NP–LC mixtures of chiral LCs. We also report on more recent research [61, 82–87] revealing potential of structures hosting lattices of defects for various applications.

In experimental studies, NPs of different mass concentrations

$$\chi = \frac{m_{NP}}{m_{NP} + m_{LC}} \tag{6}$$

having different characteristic linear size, shape and surface functionalization were used. Here, m_{NP} and m_{LC} stand for the total masses of NPs and LC molecules in the samples. The mass concentration is related to the volume concentration in the diluted regime ($p << 1$) by $\chi \approx p\frac{\rho_{NP}}{\rho_{LC}}$. Here, ρ_{NP} and ρ_{LC} stand for mass densities of NPs and LCs, respectively. Particles were either spherical (CdSe, CdSSe and Au NPs) [52–54, 76, 78, 79] or strongly anisotropic (graphene oxide, laponite and MoS_2

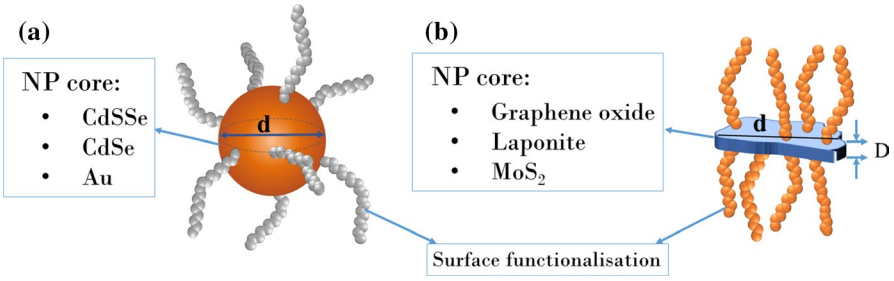

Fig. 8 A schematic representation of NPs used in experiments [52, 53, 57, 58, 78–80]. Spherical NP (CdSe, CdSSe, Au) with core diameter d (a) and anisotropic NP (graphene oxide, laponite and MoS_2 nanosheet) with average longitudinal (plate) nanosheet dimension and thickness D (b) are surface-functionalized with flexible molecules in order to prevent aggregation

Table 1 Typical NPs used in experimental studies [52–54, 57, 58, 78–80] are listed in this table

Shape	Core	Diameter (d)	Thickness (D)
Spherical	CdSSe	3.4	
Spherical	CdSe	3.5	
Spherical	Au	10	
Nanosheet	Graphene oxide	50	3–5
Nanosheet	Laponite	25	2
Nanosheet	MoS_2	10	1

Dimension d denotes the diameter of spherical NPs or the average longitudinal (plate) nanosheet dimension, while D is the thickness of the latter (as schematically depicted in Fig. 8)

nanosheets) [57, 58, 80]. Their main geometrical characteristics are schematically depicted in Fig. 8 and summarized in Table 1. Different surface functionalizations were used to prevent the aggregation of NPs and to improve their adaptivity to defect cores. The latter is schematically illustrated in Fig. 9, where a surface-decorated NP is trapped within the core of a disclination (line defect in orientational order, Fig. 9a) and a screw dislocation (line defect in translational order, Fig. 9b). Note that the structures of these defects are completely different. The nematic order is strongly distorted and, consequently, exhibits a strongly biaxial order within the disclination core. On the contrary, the nematic ordering field is relatively slightly distorted, and the smectic order is melted within the core due to the mismatch in the layer structure. However, the immersed NP is well accommodated to both (strongly different) nematic molecular field environments due to its flexible coating.

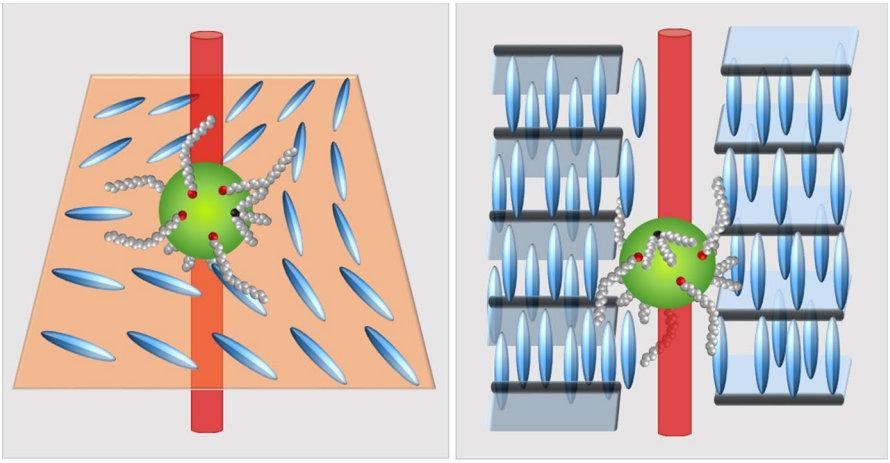

Fig. 9 Illustrations of trapped adaptive spherical NPs within a disclination (a) surrounded by nematic order and a screw dislocation (b) among adjacent slabs of smectic ordering. The adaptive character is enabled by the flexible molecules covering the NPs surface

The phase transition behavior of the mixtures was measured by high-resolution ac calorimetry [52–54]. In its principal mode of operation, so-called ac mode, this method yields with precision the temperature dependence of heat capacity C_p in case of 2nd order (continuous) transitions. In case of 1st order (discontinuous) transitions additional runs are performed using the relaxation mode; the comparison of the data obtained by the two modes can be used for the determination of latent heat.

In Fig. 10, the specific heat C_p temperature response of chiral LC compound CE8 is plotted in common scale with one concentration χ of spherical Au NPs. The bulk LC exhibits the phase sequence *I*–BPIII–BPII–BPI–N^*–Sm*A* on decreasing. One sees that for $\chi = 0.0005$ the BPIII-I phase transition exhibits the bulk-like behavior and the phase transition temperature is increased. Therefore, for small such concentrations NPs have only quantitative impact on LC behavior due to the DCR mechanism (i.e., reduced condensation penalties to form the lattice of disclinations). Furthermore, one sees that spherical NPs stabilize BPIII phase with respect to the competing BPII and BPI structures. Namely, NPs are essentially non-uniformly distributed within the space of disclination lines. Such random character stabilizes the amorphous BPIII structure with respect to ordered BPI and BPII structures. This behavior is typically observed also for other chiral LCs displaying BPs when doped with spherically shaped NPs, exhibiting the DCR mechanism. For example, in CE8 + CdSe mixtures [54] the I–BPIII transition is bulk-like even till $\chi = 0.2$. Relatively small CdSe concentrations ($\chi \sim 0.02$) are enough to suppress the stability of the BPII phase, which exists in pure samples. In such mixtures, the stability range

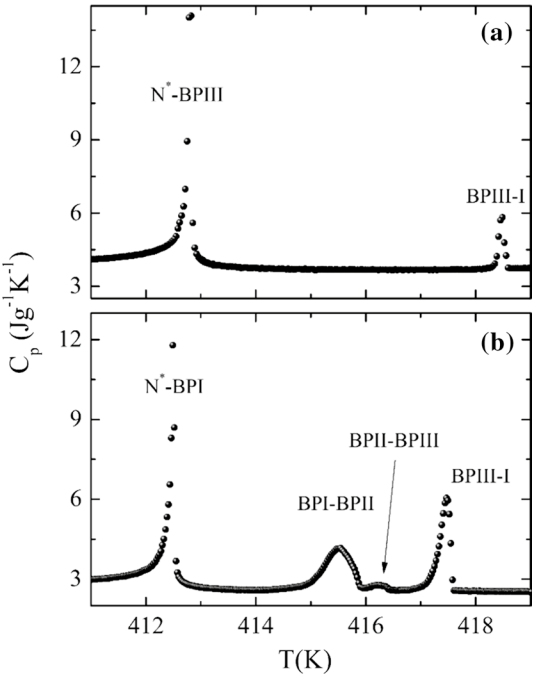

Fig. 10 The heat capacity temperature profiles $C_p(T)$, obtained by ac calorimetry, are shown for (a) mixture of CE8 with spherical Au NPs ($\chi = 0.0005$) and (b) pure CE8 from Ref. [52]

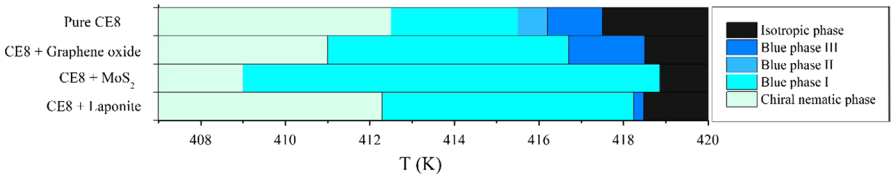

Fig. 11 The influence of surface-functionalized anisotropic NPs (graphene oxide, MoS_2, laponite) on the stability of BPs for CE8. In all cases the BPI structure is mainly stabilized over the other competing phases [57, 58, 80]

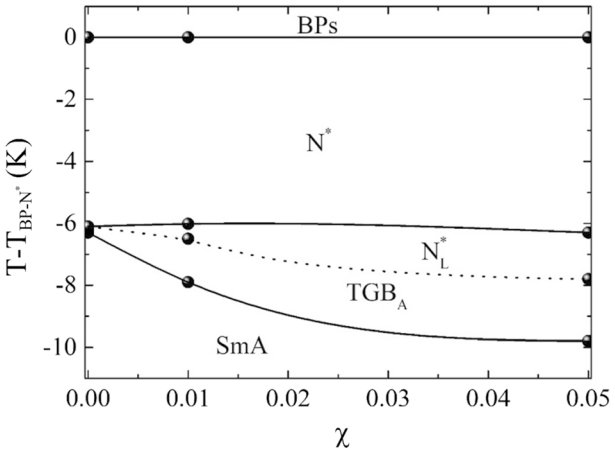

Fig. 12 Concentration–temperature phase diagram in mixtures of CE8 and CdSSe NPs

of the BPIII phase increases strongly and monotonically with χ. For example, at $\chi \sim 0.02$ the phase range is close to 10 K, while at $\chi \sim 0.2$ it extends to roughly 20 K.

The impact of various types of anisotropic NPs (nanosheets) such as graphene oxide, MoS_2 and laponite on blue phase range of CE8 is shown in Fig. 11 [57, 58, 80]. Such NPs favor the structure of BPI. For example, for a high enough concentration of MoS_2 NPs only relatively ordered body-centered cubic BPI lattice structure is stable, whose temperature stability window is increased by a factor of three times (see Fig. 11) even for moderate concentrations. Therefore, while appropriate surface-decorated spherical NPs favor the amorphous BPIII structure [52, 54], nanosheets more efficiently stabilize the more ordered BPI structure [57, 58, 61, 64, 80]. In the case of spherical small NPs, it is expected that the latter aggregate in the cores of defects. However, for essentially larger nanosheets used in [57, 58, 61, 64, 80], only a part of NPs could reside within cores of TDs. To elucidate the different impacts of spherical and anisotropic NPs on BPs structure, further systematic theoretical studies and numerical simulations are needed.

We next focus on the impact of NPs on the TGB_A phase stability [78, 79]. Note, that CE8 does not possess a stable TGB_A phase and recent studies indicate that it is close to the N^*–TGB_A–Sm*A* triple point [81]. Figure 12 illustrates that

finite concentrations χ nucleate and stabilize the TGB_A and the N_L^* phases. One sees that the temperature stability window ΔT_{TGB}^{NP} of the TGB_A and N_L^* monotonically increases on increasing χ for CdSSe NPs. In addition, it is clear that ΔT_{TGB}^{NP} monotonically increases. Furthermore, the same surface-treated NPs (e.g., CdSe quantum dots [76]) stabilize both lattices of disclinations (BPs) and dislocations (TGB_A and N_L^*), similar to what was observed in case of smaller quantum dots [76]. Note that the cores of disclinations and dislocations are significantly different, as shown in Fig. 9. Namely, within disclinations the nematic director field is strongly distorted, and the nematic order is melted (i.e., it is essentially biaxial [26]). On the contrary, the nematic director field within screw dislocations is roughly aligned along the line defect orientation, and the smectic layer order is locally melted. Therefore, to stabilize both kind of defects NPs should decrease local melting penalty required by TDs, relatively weakly distort the surrounding nematic director field in line with the DCR mechanism.

These studies illustrate that stability of TGB_A and specific BP phases could be stabilized by using appropriate NPs. Furthermore, more recent studies show that BPs doped with specific NPs, colloids, isotropic fluids or polymers gain, in addition to enhanced stability, improved or even new properties and functionalities. It was demonstrated that doping with inorganic perovskite quantum dots [87], fullerenes (C_{60}) [85], graphene oxide [61], colloidal particles [82], BPs mixed with appropriate polymers [84] or isotropic fluids [86], or dispersed in aqueous solutions [83] are of for potential use in numerous applications. For example, they could be implemented in designing switchable, multistable optical materials [82, 86], biological sensors [83], fast switching LC displays [84], as a new class of promising photorefractive liquid-crystalline materials [85], multifunctional display materials and tunable band-gap lasers [87].

5 Conclusions

In this work, we have considered the NP-driven stabilization of lattices of topological line-defect structures in LCs. Such defect configurations are spontaneously formed in the structures BPs [33, 38] and TGB_A [16, 71] phases. By using appropriate NPs the stability range of these configurations could be significantly broadened [52, 54, 76, 79], or even induced [76] if they are absent in bulk LCs. We have focused on the stabilization effect driven by the combination of DCR [46, 52] and ADCT [76] mechanisms.

Experiments reveal that size, shape and surface treatment of NPs play an important role in these phenomena. For example, our preliminary results indicate that surface-treated spherical Au NPs [79] efficiently stabilize simultaneously $m = -1/2$ disclinations lattice in BPIII and screw dislocations in TGB_A and N_L^* phases. The effective radius of surface-treated NPs was in these studies comparable to the characteristic size of disclinations and dislocations, which is determined by the nematic and smectic amplitude order parameter correlation length. In such cases, NPs are efficient in replacing the more energetically costly defect core volume with

their volume, which is the essence of the DCR mechanism. Moreover, NPs stabilize structures hosting TDs if they rather weakly perturb the (symmetry-breaking) order parameter field surrounding cores of TDs. However, NP–LC coupling should be sufficiently strong to target efficiently NPs to the cores of TDs if they are initially homogeneously dispersed in a LC body (e.g., in the isotropic phase, where the ordering fields characterizing LC structures are absent, i.e., melted). This is the essence of the ADCT mechanism. Note that spherical NPs stabilize the amorphous BPIII structure [52, 54] with respect to relatively ordered BPI and BPII disclination lattices. In this case, the effective isotropic symmetry of NPs and BPIII are more compatible with respect to other configurations. On the other hand, surface-decorated anisotropic NPs [57, 58, 61, 80] (e.g., graphene, MoS_2, laponite platelets…) stabilize BPI with respect to BPIII and BPII structures. For such cases, one of the NP's characteristic lengths is much larger than the core width of TDs. Consequently, some other stabilizing mechanisms might play an essential role in stabilizing BPI (e.g., compatibility of NP and specific BP local geometry, leading to stabilization of disclination-imposed LC structure). Additional evidence for this comes out of the fact that anisotropic NPs seem to be less (or even not) efficient in stabilizing structures possessing lattices of screw dislocations, suggesting the non-universal character of the BPI-stabilizing mechanism. On the contrary, the DCR and ADCT mechanisms are expected to be universal. Namely, the DCR mechanism is related to the condensation penalty of locally melting the amplitude field, and the ADCT mechanism to weak enough distortions in the symmetry-breaking field of the relevant order parameter describing the phase hosting a lattice of line defects.

In the presented studies, the line defect configurations were imposed via the inherent chirality of LC molecules. However, several recent studies reveal various alternative mechanisms that could be exploited to stabilize the diverse TD-patterns in LCs. For example, different configurations of disclinations could be topologically enforced via appropriately treated surfaces confining a LC phase [88–90]. Furthermore, the curvature [91–94] of LC confining substrates could be exploited to generate a rich diversity of defect configurations. Finally, a variety of defect patterns could be enforced in LC matrices via immersed NPs or colloidal particles that are relatively strongly coupled to the symmetry-breaking order parameter field component [95–102]. Such objects act effectively as TDs if they exhibit a non-toroidal topology. Consequently, they trigger additional TDs in the surrounding LC matrix in order to obey topological charge conservation rules. The resulting defect configurations could be efficiently manipulated by external electric or magnetic fields, laser beams, or LC chirality.

To summarize, interactions between diverse NPs and different TDs can stabilize and also modulate structures exhibiting lattices of TDs either in orientational or translational LC order. Diverse possible combinations of NPs and defect lattices open platforms for new applications in electro-optic, information transfer, memory storage, or sensor applications. For example, the resulting structures exhibit periodicity on the visible wavelength scale. For appropriate lattice parameters, they exhibit the bandgap structure in the visible electromagnetic spectrum. Consequently, such materials could play the role of "light semiconductors" [103–105], similar to the role of silicon in semiconductors for the electric current. Therefore, by

appropriate manipulation of defect structures, one could transfer phenomena, which triggered the "nineteenth century microelectronic revolution" based on "electronic semiconductors", to photonic applications relying on "light semiconductors". Furthermore, NPs could be exploited as "Trojan horses" to introduce novel material properties into systems. For instance, NPs could be carriers of magnetic dipoles, and in the case of the ferroelectric TGB phase, the resulting system would exhibit multiferroic properties [106].

Acknowledgments A.G. acknowledges the support of AD FUTURA, Public Scholarship, Development, Disability, and Maintenance Fund of the Republic of Slovenia. M.L., B.R., Z.K. and S.K. acknowledge the support of the Slovenian Research Agency Grant J1-9147 and programs P1-0125 and P1-0099. M.T. acknowledges the support of the Project PR-05015 of the Slovenian Research Agency. G.C. acknowledges the support of Project CZ.02.2.69/0.0/0.0/16 027/0008465 for Mobility of Researchers under the Operational Programme Research, Development and Education.

Appendix: Free Energy Densities-Enforced Behavior

Here, we summarize behaviors enforced by free energy densities given by Eq. 3.

The nematic condensation term $f_c^{(n)}$ enforces finite value of s if orientational order is condensated. For example, the *I–N* phase transition in non-chiral samples (or *I–N** transformation in chiral LCs) takes place at the critical temperature $T_{IN} = T_n^* + \frac{b_n^2}{4a_n c_n}$ [27]. For $T < T_{IN}$ the equilibrium nematic order parameter $s \equiv s_{eq}$ minimizing $f_c^{(n)}$ reads $s_{eq} = s_0\left(\frac{3+\sqrt{9-8r}}{4}\right)$. Here $s_0 = \frac{b_n}{2c_n}$ and $r = \frac{T-T_n^*}{T_{IN}-T_n^*}$. Note that in equilibrium it holds $f_c^{(n)}\left(T \le T_{IN}\right) < 0$ and $f_c^{(n)}\left(T > T_{IN}\right) = 0$.

Next, we consider the nematic elastic term $f_e^{(n)}$. The 1st term in Eq. 3b enforces spatially homogeneous amplitude *s*. Nematic director field configurations are determined by the remaining splay, twist, bend, and saddle-splay term in Eq. 3b, weighted by the Frank elastic constants K_1, K_2, K_3, and K_{24},, respectively.

These term favor nematic (for $q = 0$) or cholesteric (for $q \neq 0$) order for a relatively weak saddle-splay contribution. An equilibrium nematic phase is determined by $\vec{n} \equiv \vec{n}_{eq} = \vec{e}$. Here $\vec{e}$ determines a symmetry-breaking direction, which is spatially homogeneous. In the cholesteric phase, a helical structure is formed, where $\vec{n}$ is always perpendicular to the helix axis. For instance, for the helix axis along the z-axis, a cholesteric order could be described by $\vec{n}_{eq} = (\cos(qz), \sin(qz), 0)$ [19]. In equilibrium nematic and cholesteric phases it holds $f_c^{(n)} = 0$. In addition, each contribution in Eq. 3b equals to zero.

However, for a large enough value of K_{24} and $q \neq 0$, BPs could be energetically advantageous due to the saddle-splay contribution [14]. Note that in the latter contribution is locally different from zero if $\vec{n}$ twists simultaneously along two orthogonal directions, where more details are given in Ref. [14]. In these structures all Frank elastic term contribute, however it holds $f_c^{(n)} < 0$.

The smectic condensation term $f_c^{(s)}$ (Eq. 3c) enforces translational LC order for low enough temperatures. For example, for a positive value of a_s in non-chiral LCs the *N*–Sm*A* phase transition is of second order at the critical temperature $T_{NA} = T_s^*$. Other scenario are presented in [29].

Finally, we focus on the smectic elastic free energy contribution $f_e^{(s)}$, given in Eq. 3d. In the case of spatially constant smectic amplitude η it follows [29]

$$f_e^{(s)} = C_{\parallel}\eta^2\left|q_0\vec{n} - \nabla\phi\right|^2 + C_{\perp}\eta^2\left|\vec{n}\times\nabla\phi\right|^2.$$

For positive values of the smectic compressibility and smectic bend elastic constants the second term locally enforces parallel alignment of $\vec{n}$ and $\nabla\phi$ (i.e., smectic layer normal is aligned along $\vec{n}$). Let us assume that this is the case, where we set $\vec{n} = (0, 0, 1)$ and $\psi = \eta e^{\mathrm{i}qz}$, corresponding to a parallel stack of smectic layers along the z-axis exhibiting the layer distance $d = 2\pi/q$. It follows $f_e^{(s)} = C_{\parallel}\eta^2\left(q - q_0\right)^2$, enforcing the equilibrium layer spacing $d_{eq} \equiv \frac{2\pi}{q_0} = d$. Note that chirality favors $\nabla\times\vec{n} \neq 0$ which is incompatible with request $q_0\vec{n} = \nabla\phi$ (see Eq. 4). In this case of the compressibility term favors melting of the smectic order.

References

1. I.W. Hamley, Nanotechnology with soft materials. Angew. Chem. Int. Ed. **42**, 1692 (2003)
2. T. Hegmann, H. Qi, V.M. Marx, Nanoparticles in liquid crystals: synthesis, self-assembly, defect formation and potential applications. J. Inorg. Organomet. Polym. **17**, 483 (2007)
3. H.K. Bisoyi, S. Kumar, Liquid-crystal nanoscience: an emerging avenue of soft self-assembly. Chem. Soc. Rev. **40**, 306 (2011)
4. A.C. Balazs, T. Emrick, T.P. Russell, Nanoparticle polymer composites: where two small worlds meet. Science **314**, 1107 (2006)
5. M. Kleman, *Soft Matter Physics: An Introduction* (Springer Science & Business Media, New York, 2004)
6. Y.A. Garbovskiy, A.V. Glushchenko, in *Solid State Physics,* ed. by R.E. Camley, R.L. Stamps (Elsevier, Amsterdam, 2010), pp. 1–74
7. D.R. Nelson, Toward a tetravalent chemistry of colloids. Nano Lett. **2**, 1125 (2002)
8. P.P. Muhoray, Orientationally ordered soft matter: the diverse world of liquid crystals. Phys. Today **60**, 54 (2007)
9. N.D. Mermin, The topological theory of defects in ordered media. Rev. Mod. Phys. **51**, 591 (1979)
10. O.D. Lavrentovich, Topological defects in dispersed words and worlds around liquid crystals, or liquid crystal drops. Liq. Cryst. **24**, 117 (1998)
11. W.H. Zurek, Cosmological experiments in superfluid helium? Nature **317**, 505 (1985)
12. A. Hobson, There are no particles, there are only fields. Am. J. Phys. **81**, 211 (2013)
13. T.H.R. Skyrme, A unified field theory of mesons and baryons. Nucl. Phys. **31**, 556 (1962)
14. S. Meiboom, J.P. Sethna, P.W. Anderson, W.F. Brinkman, Theory of the blue phase of cholesteric liquid crystals. Phys. Rev. Lett. **46**, 1216 (1981)
15. D.C. Wright, N.D. Mermin, Crystalline liquids: the blue phases. Rev. Mod. Phys. **61**, 385 (1989)
16. S.R. Renn, T.C. Lubensky, Abrikosov dislocation lattice in a model of the cholesteric-to-smectic-A transition. Phys. Rev. A **38**, 2132 (1988)
17. J.W. Goodby, M.A. Waugh, S.M. Stein, E. Chin, R. Pindak, J.S. Patel, A new molecular ordering in helical liquid crystals. J. Am. Chem. Soc. **111**, 8119 (1989)
18. D. Andrienko, Introduction to liquid crystals. J. Mol. Liq. **267**, 520 (2018)
19. P. de Gennes, *The Physics of Liquid Crystals* (Oxford University Press, Oxford, 1995)
20. P.S. Pershan, Lyotropic liquid crystals. Phys. Today **35**, 34 (1982)
21. E.T. Samulski, Polymeric liquid crystals. Phys. Today **35**, 40 (1982)
22. P. de Gennes, An analogy between superconductors and smectics A. Solid State Commun. **10**, 753 (1972)
23. M. Kleman, Defects in liquid crystals. Rep. Prog. Phys. **52**, 555 (1989)

24. M.V. Kurik, O.D. Lavrentovich, Defects in liquid crystals: homotopy theory and experimental studies. Sov. Phys. Usp. **31**, 196 (1988)
25. S. Afghah, R.L.B. Selinger, J.V. Selinger, Visualising the crossover between 3D and 2D topological defects in nematic liquid crystals. Liq. Cryst. **45**, 2022 (2018)
26. N. Schopohl, T.J. Sluckin, Defect core structure in nematic liquid crystals. Phys. Rev. Lett. **59**, 2582 (1987)
27. S. Kralj, E.G. Virga, S. Žumer, Biaxial torus around nematic point defects. Phys. Rev. E **60**, 1858 (1999)
28. H. Aharoni, T. Machon, R.D. Kamien, Composite dislocations in smectic liquid crystals. Phys. Rev. Lett. **118**, 257801 (2017)
29. S. Kralj, T.J. Sluckin, Landau-de Gennes theory of the core structure of a screw dislocation in smectic A liquid crystals. Liq. Cryst. **18**, 887 (1995)
30. M. Ambrožič, S. Kralj, T.J. Sluckin, S. Žumer, D. Svenšek, Annihilation of edge dislocations in smectic-A liquid crystals. Phys. Rev. E **70**, 051704 (2004)
31. F. Reinitzer, Beiträge zur kenntniss des cholesterins. Monatsh. Chem. **9**, 421 (1888)
32. H.J. Coles, M.N. Pivnenko, Liquid crystal 'blue phases' with a wide temperature range. Nature **436**, 997 (2005)
33. S.P. James, Theory of the blue phases of chiral nematic liquid crystals. in *Theory of the Blue Phases of Chiral Nematic Liquid Crystals* (Springer, Berlin, 1987), pp. 305–324
34. I. Dierking, W. Blenkhorn, E. Credland, W. Drake, R. Kociuruba, B. Kayser, T. Michael, Stabilising liquid crystalline blue phases. Soft Matter **8**, 4355 (2012)
35. E.P. Koistinen, P.H. Keyes, Light-scattering study of the structure of blue phase III. Phys. Rev. Lett. **74**, 4460 (1995)
36. E. Dubois-violette, B. Pansu, P. Pieranski, Infinite periodic minimal surfaces: a model for blue phases. Mol. Cryst. Liq. Cryst. Inc. Nonlinear Opt. **192**, 221 (1990)
37. J. Yan, L. Rao, M. Jiao, Y. Li, H.C. Cheng, S.T. Wu, Polymer-stabilized optically isotropic liquid crystals for next-generation display and photonics applications. J. Mater. Chem. **21**, 7870 (2011)
38. S. Meiboom, M. Sammon, Structure of the blue phase of a cholesteric liquid crystal. Phys. Rev. Lett. **44**, 882 (1980)
39. O. Henrich, K. Stratford, M.E. Cates, D. Marenduzzo, Structure of blue phase III of cholesteric liquid crystals. Phys. Rev. Lett. **106**, 107801 (2011)
40. E. Kemiklioglu, J.Y. Hwang, L.C. Chien, Stabilization of cholesteric blue phases using polymerized nanoparticles. Phys. Rev. E **89**, 042502 (2014)
41. W. Cao, A. Muñoz, P.P. Muhoray, B. Taheri, Lasing in a three-dimensional photonic crystal of the liquid crystal blue phase II. Nat. Mater. **1**, 111 (2002)
42. J.P. Lagerwall, G. Scalia, A new era for liquid crystal research: applications of liquid crystals in soft matter nano-bio and microtechnology. Curr. Appl. Phys. **12**, 1387 (2012)
43. Y. Hisakado, H. Kikuchi, T. Nagamura, T. Kajiyama, Large electro-optic Kerr effect in polymer-stabilized liquid-crystalline blue phases. Adv. Mater. **17**, 96 (2005)
44. H. Iwamochi, A. Yoshizawa, Electro-optical switching in blue phases induced using a binary system of a T-shaped nematic liquid crystal and a chiral compound. Appl. Phys. Express **1**, 111801 (2008)
45. H.Y. Liu, C.T. Wang, C.Y. Hsu, T.H. Lin, J.H. Liu, Optically tuneable blue phase photonic band gaps. Appl. Phys. Lett. **96**, 121103 (2010)
46. H. Kikuchi, M. Yokota, Y. Hisakado, H. Yang, T. Kajiyama, Polymer-stabilized liquid crystal blue phases. Nat. Mater. **1**, 64 (2002)
47. G.P. Alexander, J.M. Yeomans, Stabilizing the blue phases. Phys. Rev. E **74**, 061706 (2006)
48. A. Yoshizawa, H. Iwamochi, S. Segawa, M. Sato, The role of a liquid crystal oligomer in stabilizing blue phases. Liq. Cryst. **34**, 1039 (2007)
49. H. Yoshida, Y. Tanaka, K. Kawamoto, H. Kubo, T. Tsuda, A. Fujii, S. Kuwabata, H. Kikuchi, M. Ozaki, Nanoparticle-stabilized cholesteric blue phases. Appl. Phys. Express **2**, 121501 (2009)
50. S. Taushanoff, K. Van Le, J. Williams, R.J. Twieg, B.K. Sadashiva, H. Takezoe, A. Jákli, Stable amorphous blue phase of bent-core nematic liquid crystals doped with a chiral material. J. Mater. Chem. **20**, 5893 (2010)
51. K.M. Chen, S. Gauza, H. Xianyu, S.T. Wu, Submillisecond gray-level response time of a polymer-stabilized blue-phase liquid crystal. J. Disp. Technol. **6**, 49 (2010)

52. E. Karatairi, B. Rožič, Z. Kutnjak, V. Tzitzios, G. Nounesis, G. Cordoyiannis, J. Thoen, C. Glorieux, S. Kralj, Nanoparticle-induced widening of the temperature range of liquid-crystalline blue phases. Phys. Rev. E **81**, 041703 (2010)
53. G. Cordoyiannis, P. Losada-Pérez, C.S.P. Tripathi, B. Rožič, U. Tkalec, V. Tzitzios, E. Karatairi, G. Nounesis, Z. Kutnjak, I. Muševič, Blue phase III widening in CE6-dispersed surface-functionalised CdSe nanoparticles. Liq. Cryst. **37**, 1419 (2010)
54. B. Rožič, V. Tzitzios, E. Karatairi, U. Tkalec, G. Nounesis, Z. Kutnjak, G. Cordoyiannis, R. Rosso, E.G. Virga, I. Muševič, Theoretical and experimental study of the nanoparticle-driven blue phase stabilization. Eur. Phys. J. E **34**, 17 (2011)
55. H. Choi, H. Higuchi, Y. Ogawa, H. Kikuchi, Polymer-stabilized supercooled blue phase. Appl. Phys. Lett. **101**, 131904 (2012)
56. L. Wang, W. He, X. Xiao, F. Meng, Y. Zhang, P. Yang, L. Wang, J. Xiao, H. Yang, Y. Lu, Hysteresis-free blue phase liquid-crystal-stabilized by ZnS nanoparticles. Small **8**, 2189 (2012)
57. M. Lavrič, V. Tzitzios, S. Kralj, G. Cordoyiannis, I. Lelidis, G. Nounesis, V. Georgakilas, H. Amenitsch, A. Zidanšek, Z. Kutnjak, The effect of graphene on liquid-crystalline blue phases. Appl. Phys. Lett. **103**, 143116 (2013)
58. M. Lavrič, G. Cordoyiannis, S. Kralj, V. Tzitzios, G. Nounesis, Z. Kutnjak, Effect of anisotropic MoS_2 nanoparticles on the blue phase range of a chiral liquid crystal. Appl. Opt. **52**, 47 (2013)
59. I. Gvozdovskyy, 'Blue phases' of highly chiral thermotropic liquid crystals with a wide range of near-room temperature. Liq. Cryst. **42**, 1391 (2015)
60. M.A. Gharbi, S. Manet, J. Lhermitte, S. Brown, J. Milette, V. Toader, M. Sutton, L. Reven, Reversible nanoparticle cubic lattices in blue phase liquid crystals. ACS Nano **10**, 3410 (2016)
61. W. Zhang, X. Wang, D. Wang, Z. Yang, H. Gao, Y. Xing, W. He, H. Cao, H. Yang, Blue phase liquid crystals affected by graphene oxide modified with aminoazobenzol group. Liq. Cryst. **43**, 573 (2016)
62. S.Y. Jo, S.W. Jeon, B.C. Kim, J.H. Bae, F. Araoka, S.W. Choi, Polymer stabilization of liquid-crystal blue phase II toward photonic crystals. ACS Appl. Mater. Interfaces **9**, 8941 (2017)
63. F. Liu, G. Ma, D. Zhao, Nickel nanoparticle-stabilized room-temperature blue-phase liquid crystals. Nanotechnology **29**, 285703 (2018)
64. Y. Zhao, X. Qiao, K. Li, S. Ding, S. Tian, H. Ren, M. Zhu, Q. Ma, Y. Zhao, Q. Ban, Blue phase liquid crystals stabilized by graphene oxide modified with aminoalkyl group. Mol. Cryst. Liq. Cryst. **664**, 1 (2018)
65. S.R. Renn, T.C. Lubensky, Existence of a Sm-C grain boundary phase at the chiral MAC point. Mol. Cryst. Liq. Cryst. **209**, 349 (1991)
66. S.R. Renn, Multicritical behavior of Abrikosov vortex lattices near the cholesteric–smectic-A–smectic-C* point. Phys. Rev. A **45**, 953 (1992)
67. L. Navailles, H.T. Nguyen, P. Barois, C. Destrade, N. Isaert, Smectic A twist grain boundary phase in three new series with chiral (L) lactic acid derivatives. Liq. Cryst. **15**, 479 (1993)
68. L. Navailles, B. Pansu, L. Gorre-Talini, H.T. Nguyen, Structural study of a commensurate TGB A phase and of a presumed chiral line liquid phase. Phys. Rev. Lett. **81**, 4163 (1998)
69. L. Navailles, P. Barois, H.T. Nguyen, X-ray measurement of the twist grain boundary angle in the liquid crystal analog of the Abrikosov phase. Phys. Rev. Lett. **71**, 545 (1993)
70. J.W. Goodby, M.A. Waugh, S.M. Stein, E. Chin, R. Pindak, J.S. Patel, Characterization of a new helical smectic liquid crystal. Nature **337**, 449 (1989)
71. T.C. Lubensky, S.R. Renn, Twist-grain-boundary phases near the nematic–smectic-A–smectic-C point in liquid crystals. Phys. Rev. A **41**, 4392 (1990)
72. R.D. Kamien, T.C. Lubensky, Twisted line liquids. J. Phys. I **3**, 2131 (1993)
73. G. Srajer, R. Pindak, M.A. Waugh, J.W. Goodby, J.S. Patel, Structural measurements on the liquid-crystal analog of the Abrikosov phase. Phys. Rev. Lett. **64**, 1545 (1990)
74. K.J. Ihn, J.A.N. Zasadzinski, R. Pindak, A.J. Slaney, J. Goodby, Observations of the liquid-crystal analog of the Abrikosov phase. Science **258**, 275 (1992)
75. O.D. Lavrentovich, Y.A. Nastishin, V.I. Kulishov, Y.S. Narkevich, A.S. Tolochko, S.V. Shiyanovskii, Helical smectic A. Europhys. Lett. **13**, 313 (1990)
76. G. Cordoyiannis, V.S. Rao Jampani, S. Kralj, S. Dhara, V. Tzitzios, G. Basina, G. Nounesis, Z. Kutnjak, C.S. Pati Tripathi, P. Losada-Pérez, Different modulated structures of topological defects stabilized by adaptive targeting nanoparticles. Soft Matter **9**, 3956 (2013)
77. C. Kyrou, S. Kralj, M. Panagopoulou, Y. Raptis, G. Nounesis, I. Lelidis, Impact of spherical nanoparticles on nematic order parameters. Phys. Rev. E **97**, 042701 (2018)

78. M. Trček, G. Cordoyiannis, V. Tzitzios, S. Kralj, G. Nounesis, I. Lelidis, Z. Kutnjak, Nanoparticle-induced twist-grain boundary phase. Phys. Rev. E **90**, 032501 (2014)
79. M. Trček, G. Cordoyiannis, B. Rožič, V. Tzitzios, G. Nounesis, S. Kralj, I. Lelidis, E. Lacaze, H. Amenitsch, Z. Kutnjak, Twist-grain boundary phase induced by Au nanoparticles in a chiral liquid crystal host. Liq. Cryst. **44**, 1575 (2017)
80. M. Lavrič, V. Tzitzios, G. Cordoyiannis, S. Kralj, G. Nounesis, I. Lelidis, Z. Kutnjak, Blue phase range widening induced by laponite nanoplatelets in the chiral liquid crystal CE8. Mol. Cryst. Liq. Cryst. **615**, 14 (2015)
81. M. Trček, G. Cordoyiannis, Z. Kutnjak, G. Nounesis, I. Lelidis, Twist-grain-boundary-A* phase stabilisation in confined geometry by the interfaces. Liq. Cryst. **43**, 1437 (2016)
82. K. Stratford, O. Henrich, J.S. Lintuvuori, M.E. Cates, D. Marenduzzo, Self-assembly of colloid-cholesteric composites provides a possible route to switchable optical materials. Nat. Commun. **5**, 3954 (2014)
83. E. Bukusoglu, X. Wang, J.A. Martinez-Gonzalez, J.J. de Pablo, N.L. Abbott, Stimuli-responsive cubosomes formed from blue phase liquid crystals. Adv. Mater. **27**, 6892 (2015)
84. H. Kikuchi, S. Izena, H. Higuchi, Y. Okumura, K. Higashiguchi, A giant polymer lattice in a polymer-stabilized blue phase liquid crystal. Soft Matter **11**, 4572 (2015)
85. I.C. Khoo, C.W. Chen, T.J. Ho, Observation of photorefractive effects in blue-phase liquid crystal containing fullerene-C 60. Opt. Lett. **41**, 123 (2016)
86. J.S. Lintuvuori, K. Stratford, M.E. Cates, D. Marenduzzo, Mixtures of blue phase liquid crystal with simple liquids: elastic emulsions and cubic fluid cylinders. Phys. Rev. Lett. **121**, 037802 (2018)
87. P. Lin, Q. Yan, Z. Wei, Y. Chen, F. Chen, Z. Huang, X. Li, H. Wang, X. Wang, Z. Cheng, All-inorganic perovskite quantum dots stabilized blue phase liquid crystals. Opt. Express **26**, 18310 (2018)
88. B.S. Murray, R.A. Pelcovits, C. Rosenblatt, Creating arbitrary arrays of two-dimensional topological defects. Phys. Rev. E **90**, 052501 (2014)
89. H. Yoshida, K. Asakura, J. Fukuda, M. Ozaki, Three-dimensional positioning and control of colloidal objects utilizing engineered liquid crystalline defect networks. Nat. Commun. **6**, 7180 (2015)
90. Y. Sasaki, V. Jampani, C. Tanaka, N. Sakurai, S. Sakane, K.V. Le, F. Araoka, H. Orihara, Large-scale self-organization of reconfigurable topological defect networks in nematic liquid crystals. Nat. Commun. **7**, 13238 (2016)
91. M. Bowick, D.R. Nelson, A. Travesset, Curvature-induced defect unbinding in toroidal geometries. Phys. Rev. E **69**, 041102 (2004)
92. V. Vitelli, A.M. Turner, Anomalous coupling between topological defects and curvature. Phys. Rev. Lett. **93**, 215301 (2004)
93. L. Mesarec, W. Góźdź, A. Iglič, S. Kralj, Effective topological charge cancelation mechanism. Sci. Rep. **6**, 27117 (2016)
94. I.I. Smalyukh, R. Pratibha, N.V. Madhusudana, O.D. Lavrentovich, Selective imaging of 3D director fields and study of defects in biaxial smectic A liquid crystals. Eur. Phys. J. E **16**, 179 (2005)
95. D. Pires, J.B. Fleury, Y. Galerne, Colloid particles in the interaction field of a disclination line in a nematic phase. Phys. Rev. Lett. **98**, 247801 (2007)
96. U. Tkalec, M. Ravnik, S. Čopar, S. Žumer, I. Musevic, Reconfigurable knots and links in chiral nematic colloids. Science **333**, 62 (2011)
97. B. Senyuk, Q. Liu, S. He, R.D. Kamien, R.B. Kusner, T.C. Lubensky, I.I. Smalyukh, Topological colloids. Nature **493**, 200 (2013)
98. Q. Liu, B. Senyuk, M. Tasinkevych, I.I. Smalyukh, Nematic liquid crystal boojums with handles on colloidal handlebodies. Proc. Natl. Acad. Sci. **110**, 9231 (2013)
99. M. Muševič, Škarabot, Self-assembly of nematic colloids. Soft Matter **4**, 195 (2008)
100. R. Jose, G. Skačej, V.S.S. Sastry, S. Žumer, Colloidal nanoparticles trapped by liquid-crystal defect lines: a lattice Monte Carlo simulation. Phys. Rev. E **90**, 032503 (2014)
101. M. Ravnik, G.P. Alexander, J.M. Yeomans, S. Žumer, Three-dimensional colloidal crystals in liquid crystalline blue phases. Proc. Natl. Acad. Sci. **108**, 5188 (2011)
102. Y. Yuan, A. Martinez, B. Senyuk, M. Tasinkevych, I.I. Smalyukh, Chiral liquid crystal colloids. Nat. Mater. **17**, 71 (2018)
103. D. Lindley, Focus: landmarks——the birth of photonic crystals. Physics **6**, 94 (2013)
104. E. Yablonovitch, Inhibited spontaneous emission in solid-state physics and electronics. Phys. Rev. Lett. **58**, 2059 (1987)

105. D.Y. Guo, C.W. Chen, C.C. Li, H.C. Jau, K.H. Lin, T.M. Feng, C.T. Wang, T.J. Bunning, I.C. Khoo, T.H. Lin, Reconfiguration of three-dimensional liquid-crystalline photonic crystals by electrostriction. Nat. Mater. **19**, 94 (2020)
106. M. Fiebig, T. Lottermoser, D. Meier, M. Trassin, The evolution of multiferroics. Nat. Rev. Mater. **1**, 16046 (2016)